Supporting information for "Impact of updating vegetation information on land surface model performance"

Melissa Ruiz-Vásquez[1,2], Sungmin O[3], Gabriele Arduini[4], Souhail Boussetta[4],

Alexander Brenning[2], Ana Bastos[1], Sujan Koirala[1], Gianpaolo Balsamo[4],

Markus Reichstein[1], and René Orth[1]

[1]Department of Biogeochemical Integration, Max Planck Institute for Biogeochemistry, Jena, Germany

[2]Friedrich Schiller University Jena, Department of Geography, Jena, Germany

[3]Department of Climate and Energy System Engineering, Ewha Womans University, Seoul, South Korea

[4]Research Department, European Centre for Medium-Range Weather Forecasts, Reading, UK

Contents of this file **Page**

Corresponding author: M. Ruiz-Vásquez, Department of Biogeochemical Integration, Max Planck Institute for Biogeochemistry, Jena, Germany (mruiz@bgc-jena.mpg.de)

Introduction

The present document contains additional material (Table and Figures) that supports the discussion in the study "Impact of updating vegetation information on land surface model performance". This material is not included in the main text because it is not essential to the main scientific conclusins other than providing additional information.

Table S1. Land use classification in the Global Land Cover Characterization (GLCC) v1.2 according to the Biosphere-Atmosphere Transfer Scheme (BATS)

Vegetation type	**High/Low (H/L) vegetation**
Crops,mixed, farming	L
Short grass	L
Evergreen needleleaf trees	H
Deciduous needleleaf trees	H
Deciduous broadleaf trees	H
Evergreen broadleaf trees	H
Tall grass	L
Desert	–
Tundra	L
Irrigated crops	L
Semidesert	L
Ice caps and glaciers	–
Bogs and marshes	L
Inland water	–
Ocean	–
Evergreen shrubs	L
Deciduous shrubs	L
Mixed forest/woodland	H
Interrupted forest	H
Water and land mixtures	L

Table S2: Description of the selected reference datasets

Data	**Description**	**Advantages**	**Disadvantages**	**Reference**
SoMo.ml	Global long-term soil moisture dataset at multiple soil layers (0–10, 10–30 and 30–50 cm) derived through a Long Short-Term Memory (LSTM) algorithm. LSTM is trained using *in-situ* data collected through more than 1000 stations across the globe to extrapolate daily soil moisture dynamics in space and in time.	This dataset is uniformly distributed globally and represents not only the top few centimetres of the soil. It provides soil moisture information independent from the existing satellite or physical-based model data.	The data quality can be uncertain outside the training conditions such as at high latitudes and in arid regions.	O and Orth (2021)

Global Land Evaporation Amsterdam Model (GLEAM)	This is a set of algorithms that estimate terrestrial evaporation and root-zone soil moisture from satellite data. GLEAM separately derives the different components of terrestrial evaporation for different fractions of land cover types in each grid cell. Estimates of potential evaporation are converted into actual transpiration or bare soil evaporation (depending on the land-cover type). The soil moisture is calculated using a multi-layer water-balance algorithm considering net precipitation and snowmelt as inputs, and evaporation and drainage as outputs. The depth of the root zone is a function of the land-cover type.	GLEAM uses high quality forcing datasets to produce accurate model output.	The results might be biased given that the majority (more than 75%) of the *in-situ* measurements are located in the continental US, where gauge-based precipitation products are known to outperform satellite products.	Martens et al. (2017)
Modern-Era Retrospective Analysis for Research and Applications Version 2 (MERRA-2)	This is an atmospheric reanalysis of the modern satellite era produced by NASA's Global Modeling and Assimilation Office. MERRA-2 incorporates data from the atmospheric model of Goddard Earth Observing System and numerous satellite observations. The analysis is computed on a latitude-longitude grid at the same spatial resolution as the atmospheric model using a 3DVAR data assimilation.	The renalysis combines scattered observations in a physically consistent manner, enabling production of completely gridded variables.	It presents biases in some variables, especially over high topography in the tropics and over northern high latitudes.	Gelaro et al. (2017)

FLUXCOM RS	This is a machine learning-based global dataset that estimates radiation and latent and sensible heat from energy flux measurements from FLUXNET eddy covariance towers along with remote sensing data.	FLUXCOM RS does not use global climate forcing datasets as inputs, which favours the accuracy of the fluxes because such datasets are subject to uncertainty and are limited in spatial resolution.	Not using climate data excludes potentially important information on meteorological conditions for biosphere-atmosphere fluxes and limits temporal coverage to the one of MODIS.	Jung et al. (2019)

Table S3. Optimal perturbation factors for the model parameters after global calibration

Model parameter	**Optimal perturbation factors**
Hydraulic conductivity	0.09766
Humidity stress function	0.83900
Minimum stomatal resistance	1.27800
Soil moisture stress function	1.47000
Total soil depth	1.06044
Transmission of net solar radiation through vegetation	0.13652

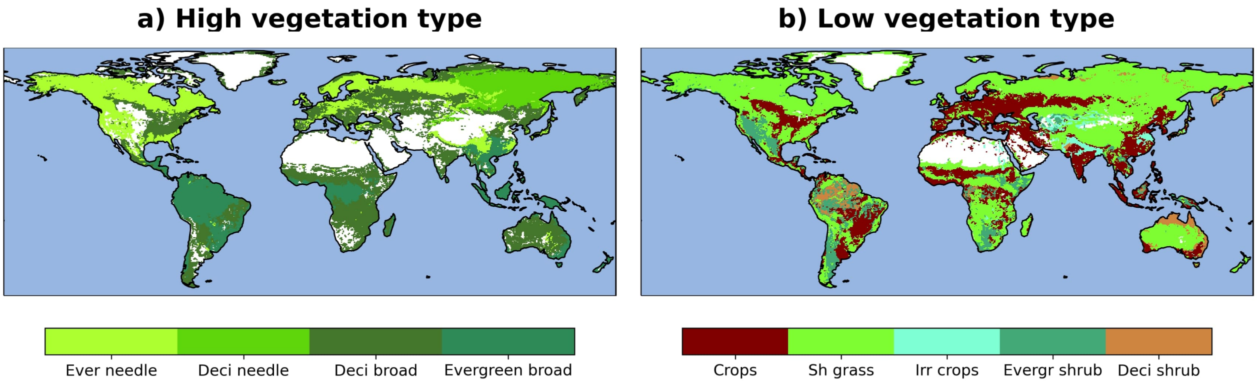

Figure S1. Updated vegetation type in ECLand for a) high vegetation and b) low vegetation. Dataset from ESA-CCI/C3S.

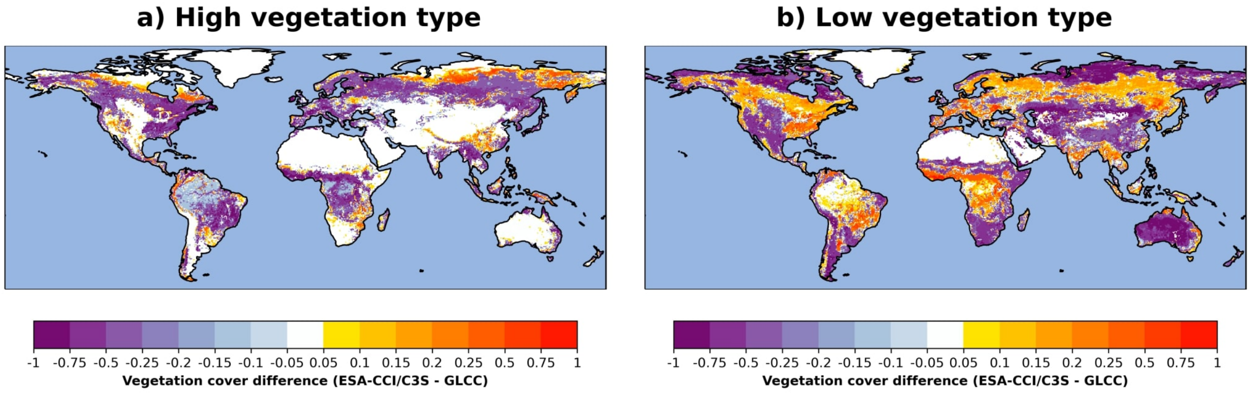

Figure S2. Vegetation cover difference (fraction) between ESA-CCI/C3S and GLCC for a) high vegetation and b) low vegetation.

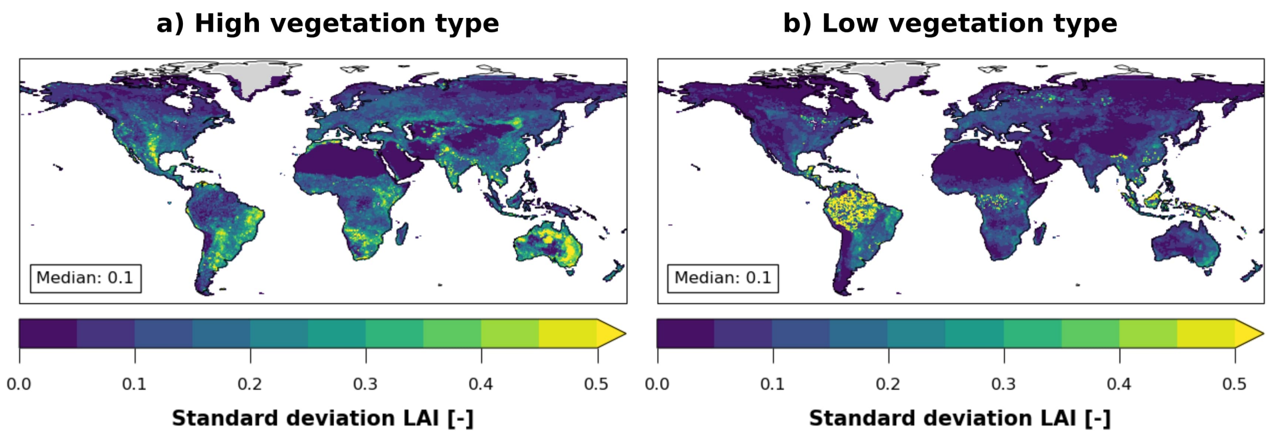

Figure S3. Standard deviation of annual mean LAI values (2000-2019) for a) high vegetation and b) low vegetation. Dataset from Sentinel-3 and THEA GEOV2.

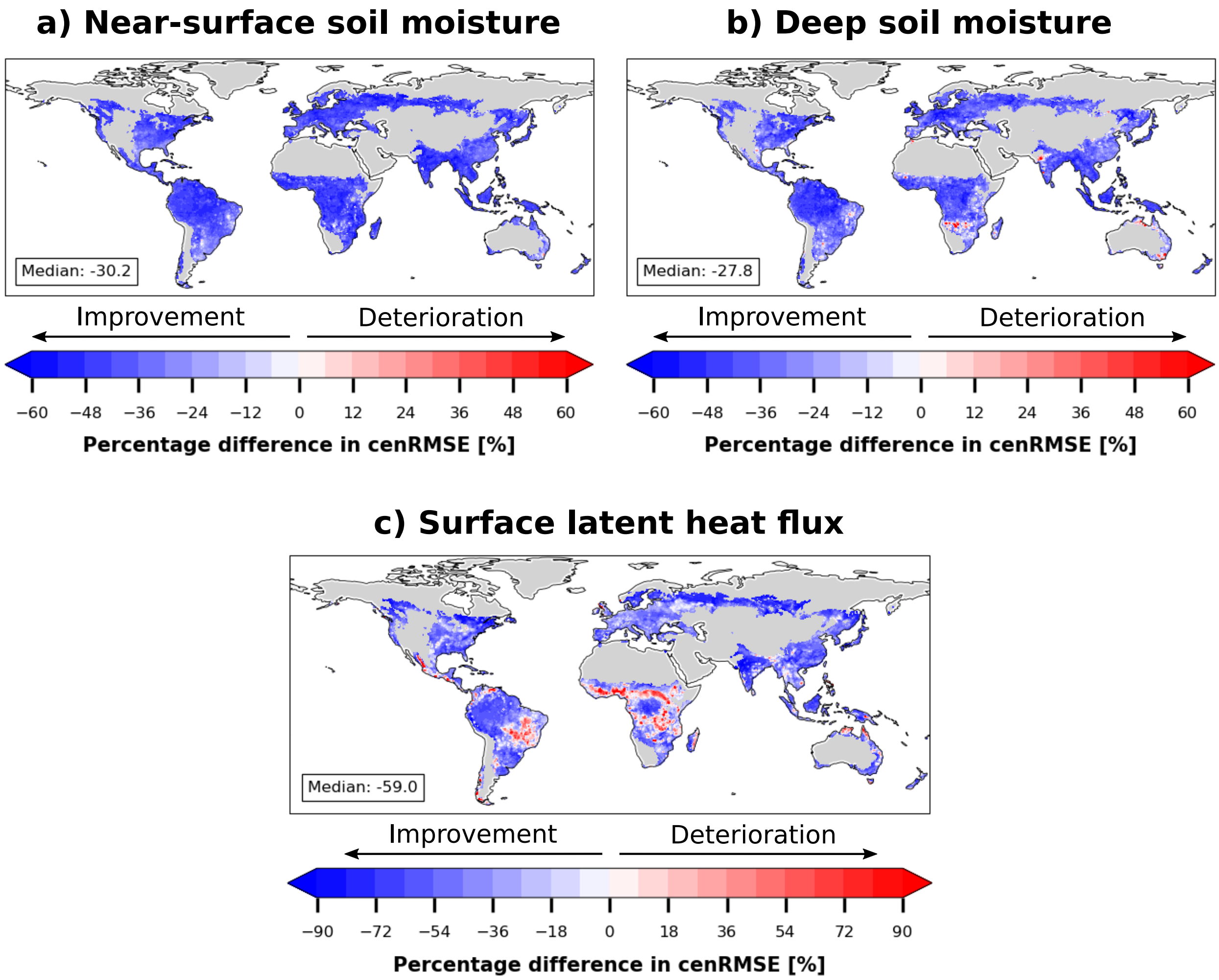

Figure S4. Percentage differences in cenRMSE model performance: LC_COV_LAI minus CONTROL divided by CONTROL for a) near-surface soil moisture, b) deep soil moisture and c) surface latent heat flux. Outliers based on the 90^{th} quantile are removed before the computation of the performance metric. Numbers in the textboxes represent the global median.

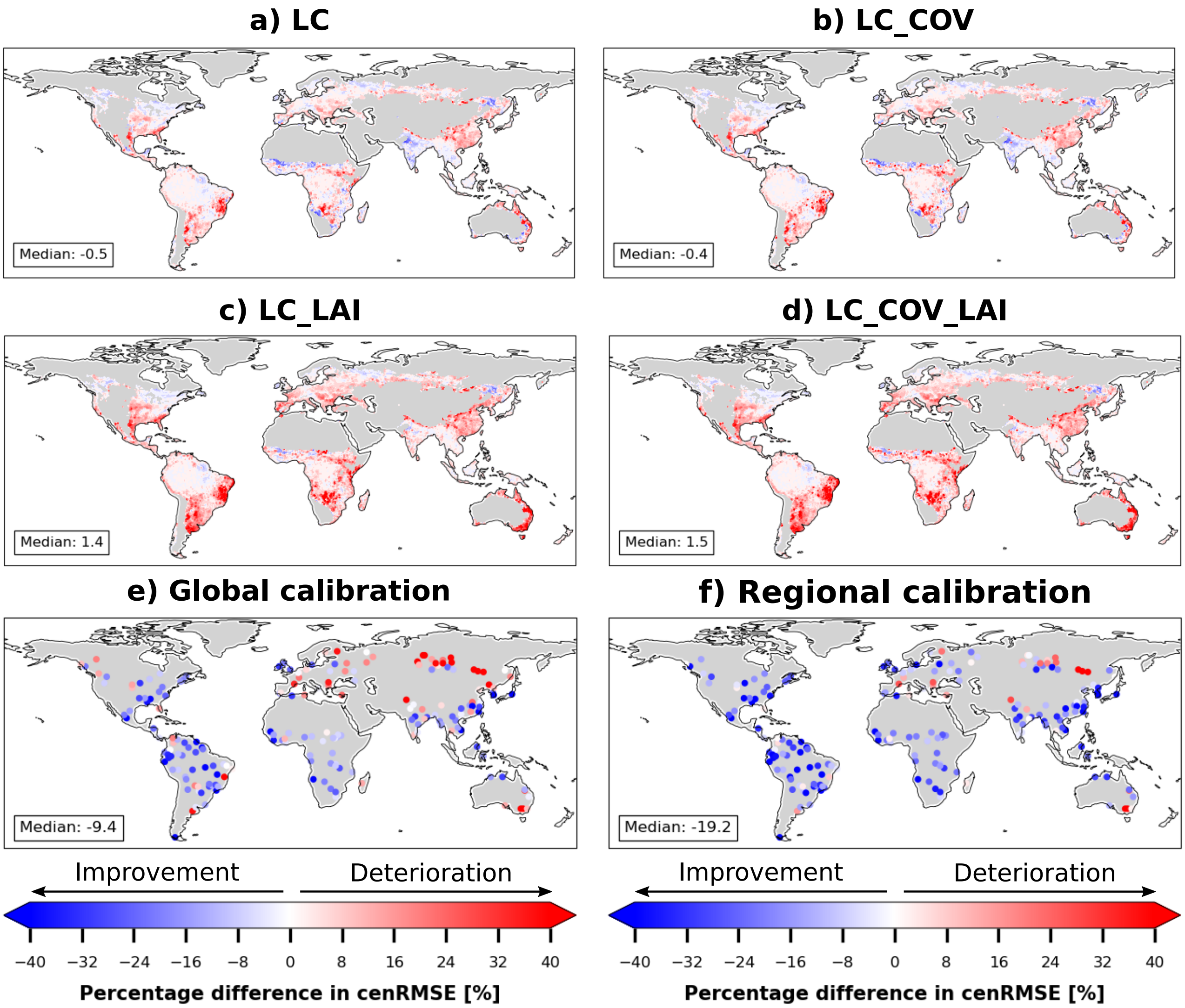

Figure S5. Percentage differences in cenRMSE model performance for near-surface soil moisture in a) LC, b) LC_COV, c) LC_LAI, d) LC_COV_LAI, e) Global calibration and f) Regional calibration simulations with regards to CONTROL simulation. Numbers in the textboxes represent the global median.

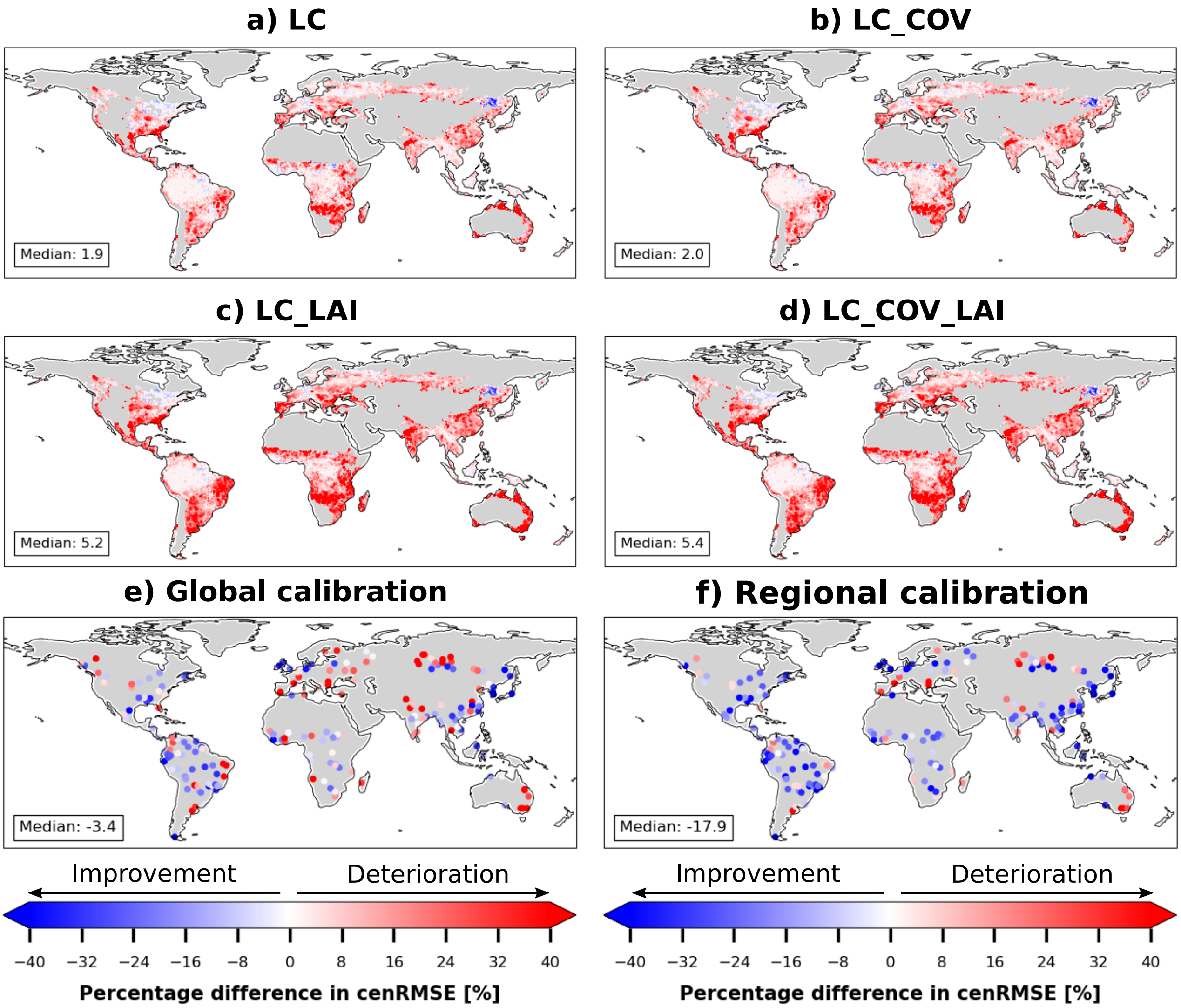

Figure S6. Similar to Figure S5, but for deep soil moisture.

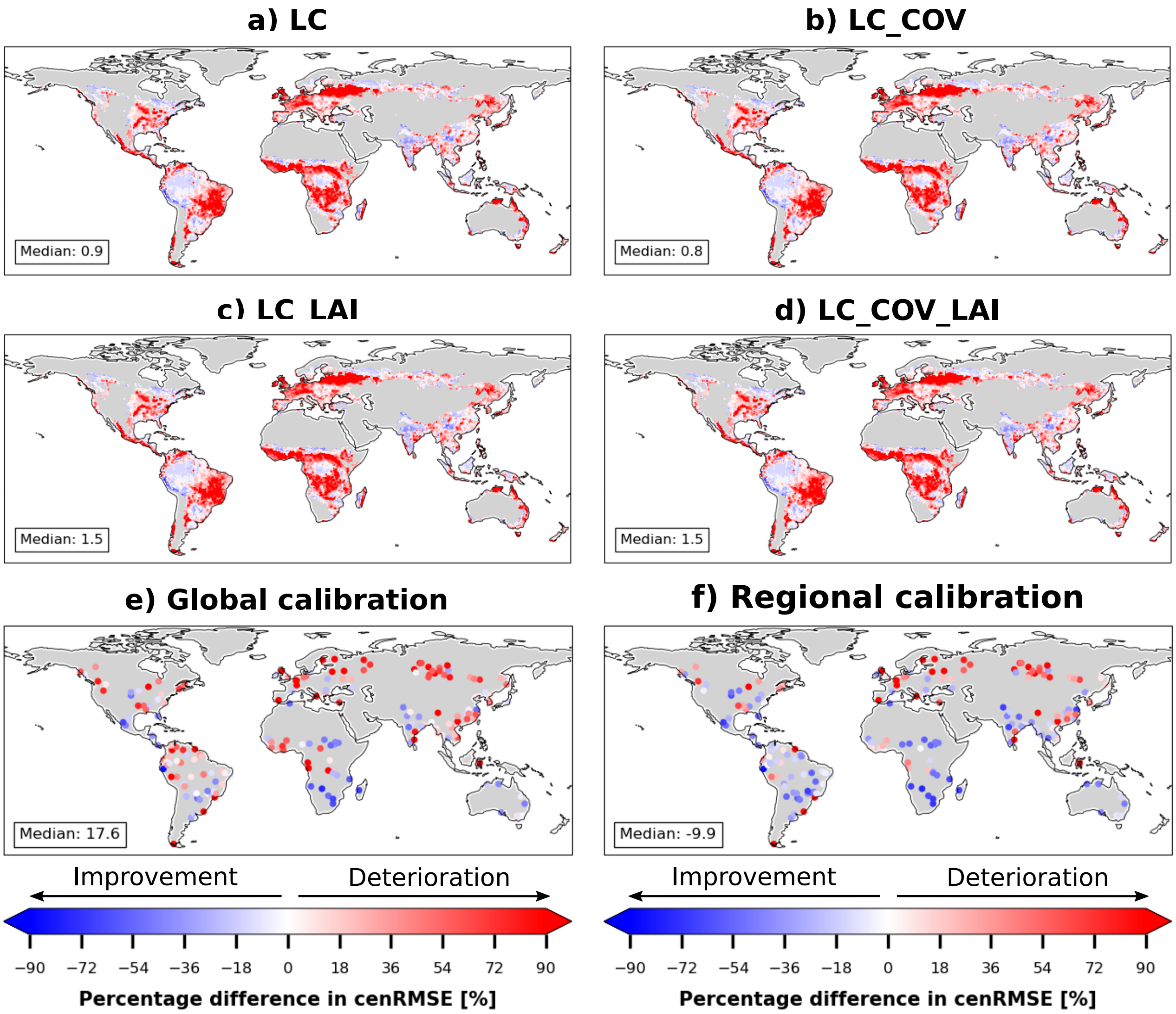

Figure S7. Similar to Figure S5, but for surface latent heat flux.

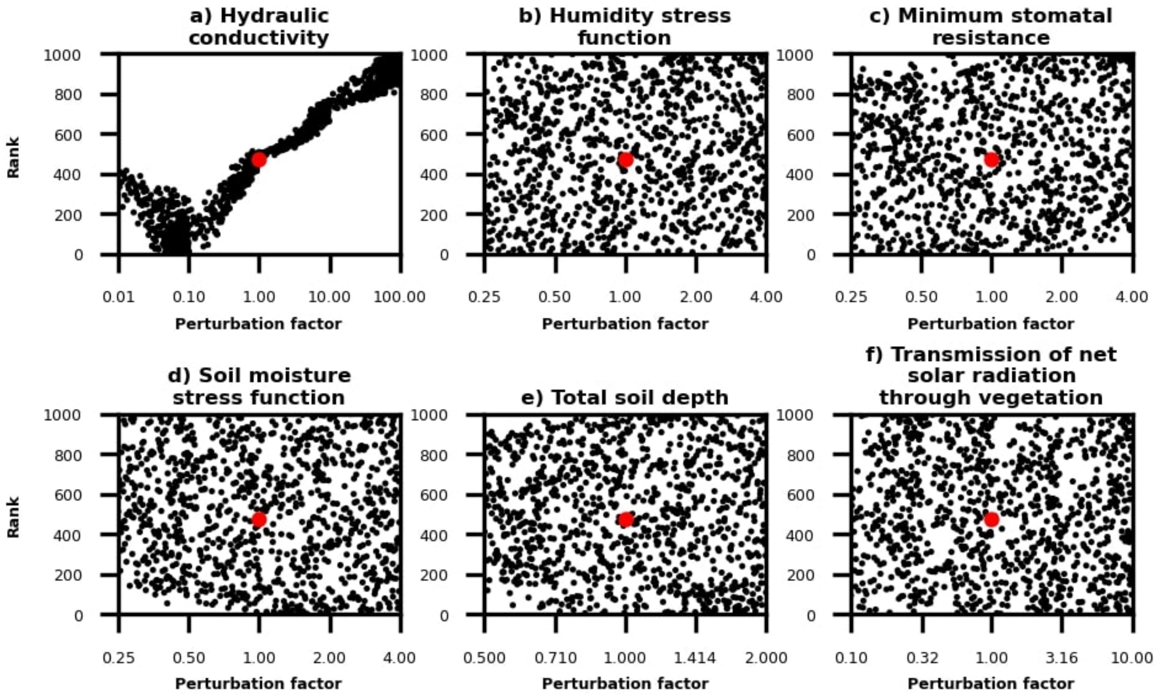

Figure S8. Rankings of 1001 random perturbation factors for near-surface soil moisture for a) hydraulic conductivity, b) humidity stress function, c) minimum stomatal resistance, d) soil moisture stress function, e) total soil depth and f) transmission of net solar radiation through vegetation. Red dots indicate the performance of the default parameterizations (i.e. no perturbation).

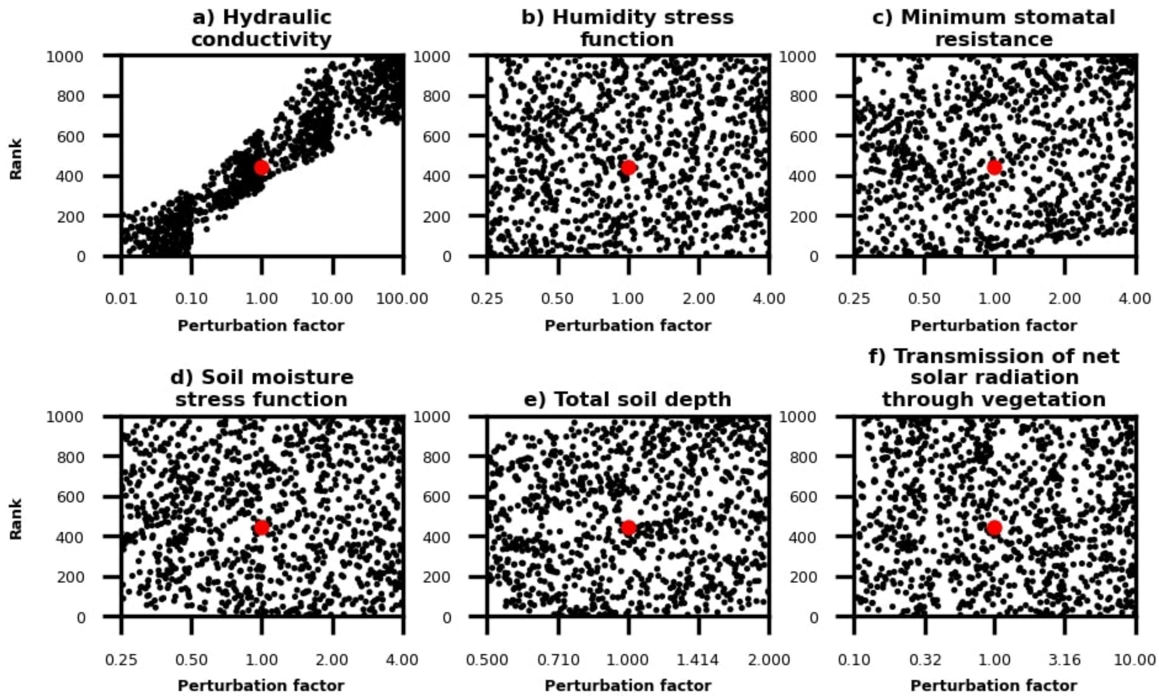

Figure S9. Similar to Figure S8, but for deep soil moisture.

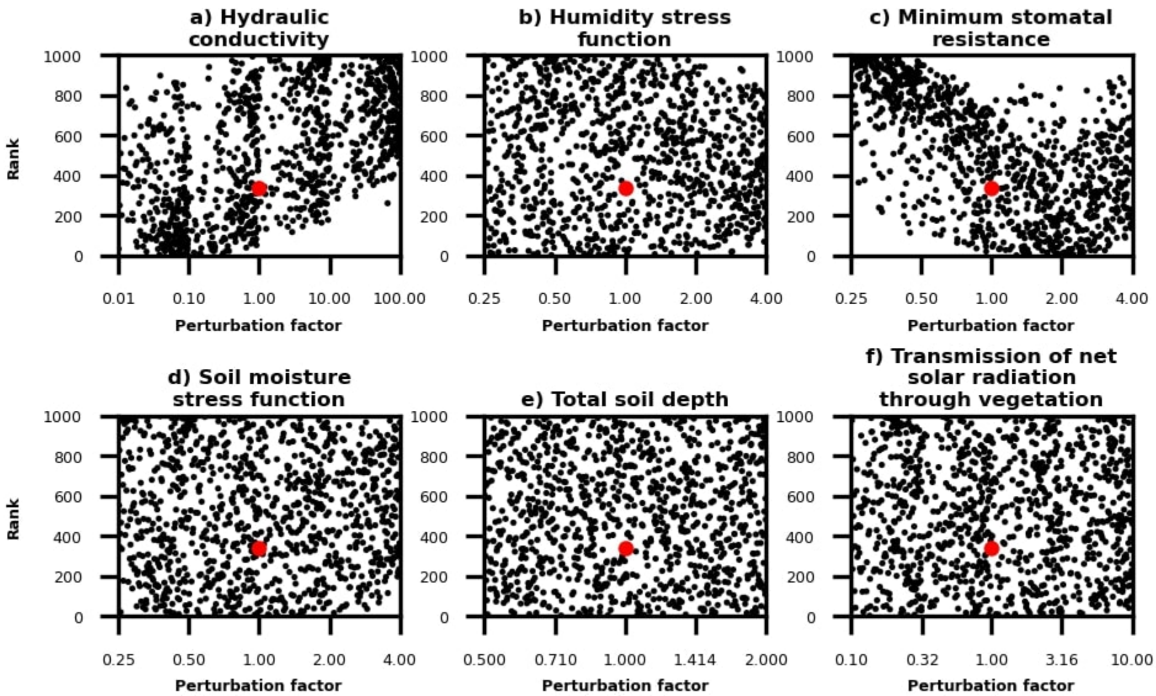

Figure S10. Similar to Figure S8, but for surface latent heat flux.

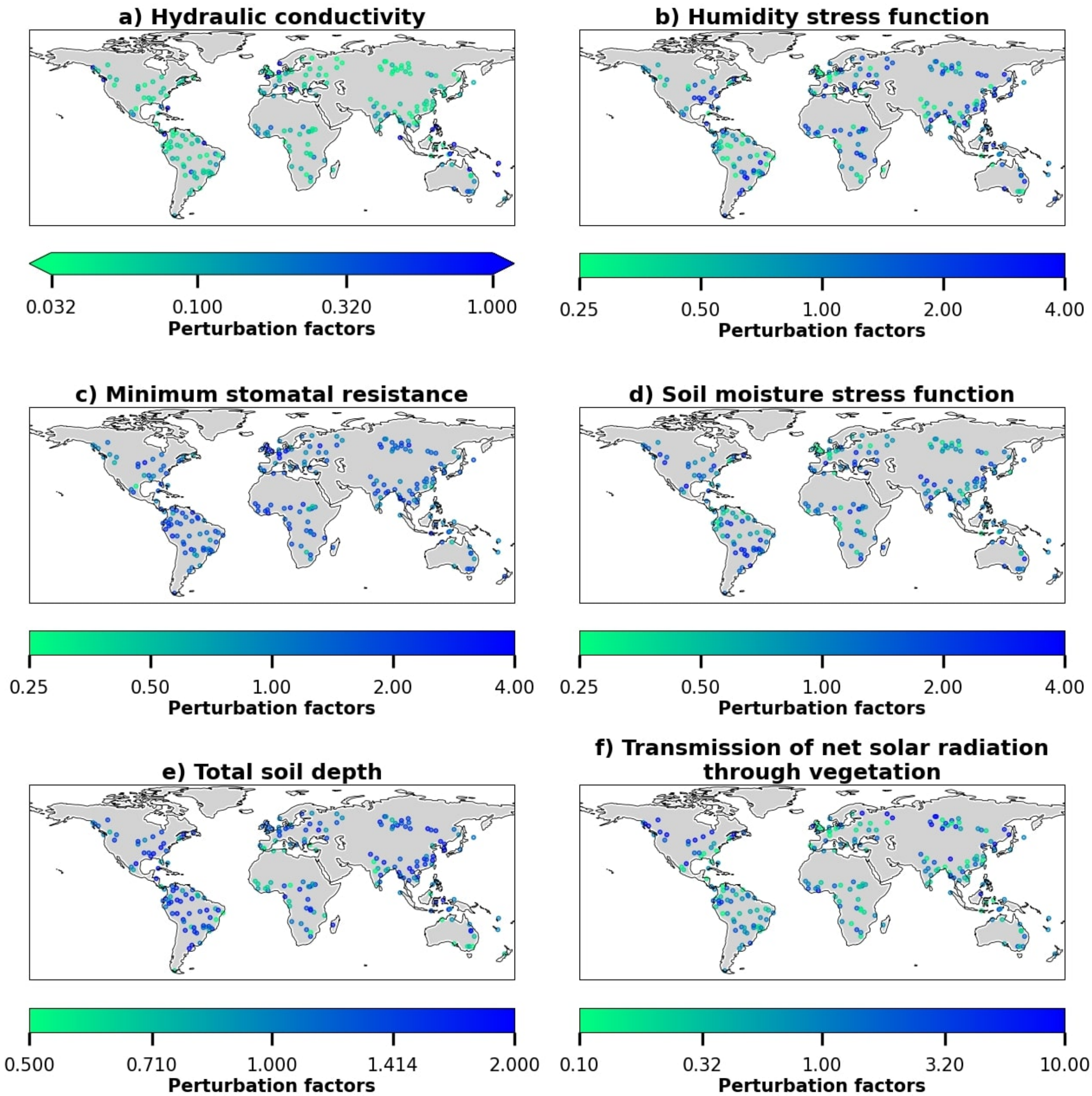

Figure S11. Spatial distribution of the calibrated parameter values in the regional calibration experiment for a) hydraulic conductivity, b) humidity stress function, c) minimum stomatal resistance, d) soil moisture stress function, e) total soil depth and f) transmission of net solar radiation through vegetation.

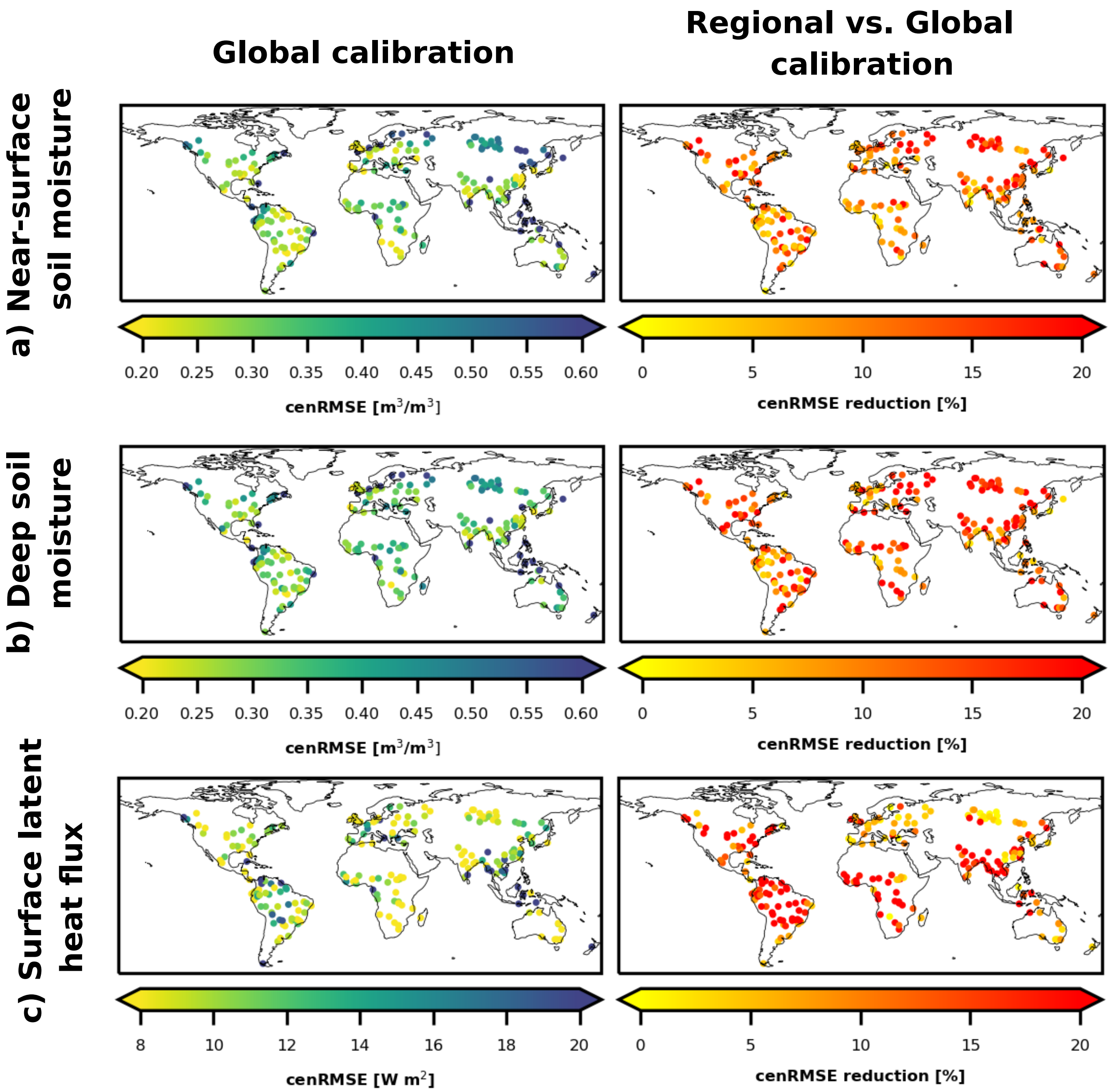

Figure S12. Model performance of the global parameter calibration experiment (left column) and reduction in cenRMSE of the regional parameter calibration experiment with regards to the global calibration experiment (right column) for a) near-surface soil moisture, b) deep soil moisture and c) surface latent heat flux.

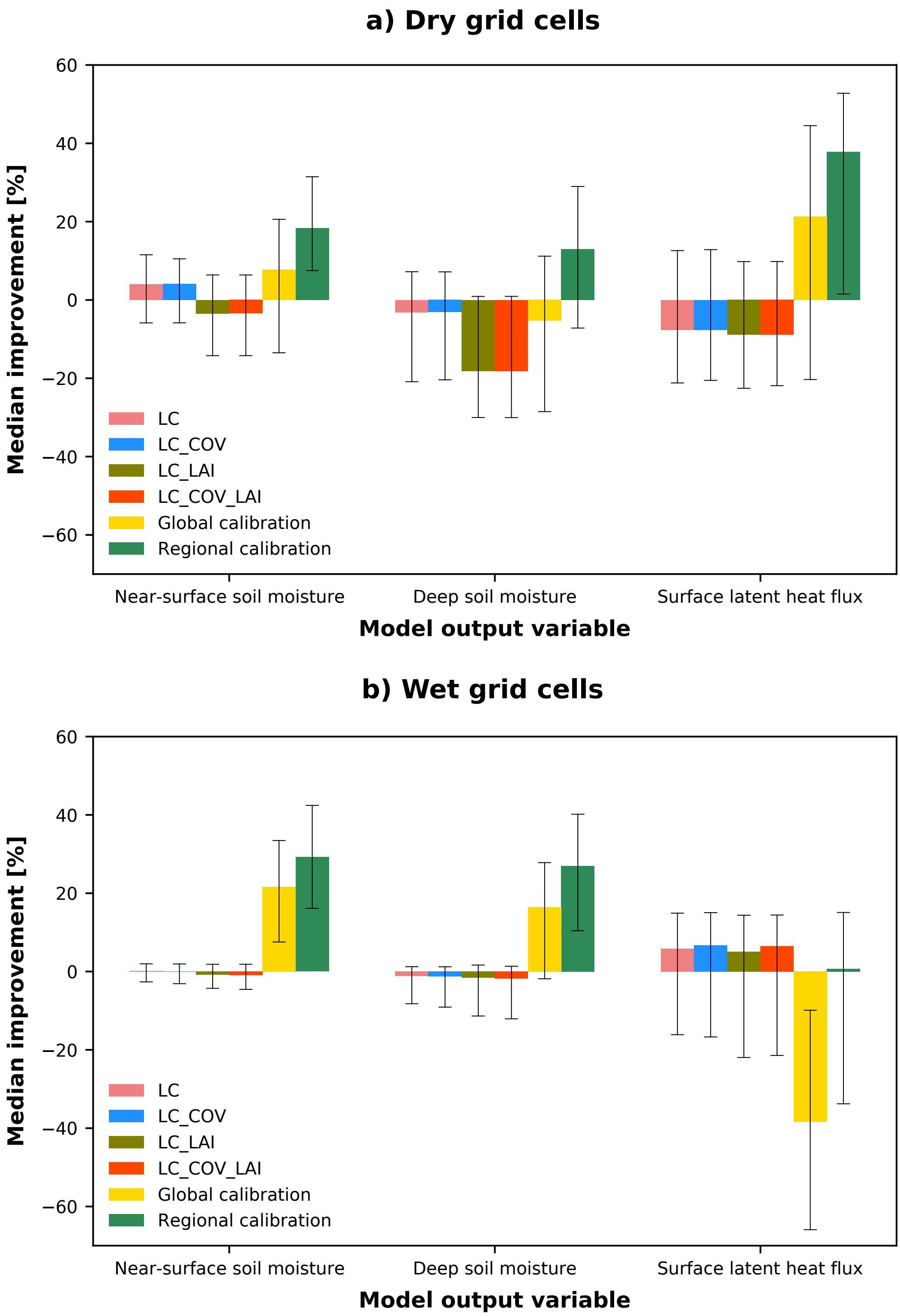

Figure S13. Summary of ECLand performance for each experiment compared to the CONTROL simulation only considering a) dry (≤first quartile of soil moisture) and b) wet (≥ third quartile of soil moisture) grid cells. The error bars represent the 25th and 75th percentile.

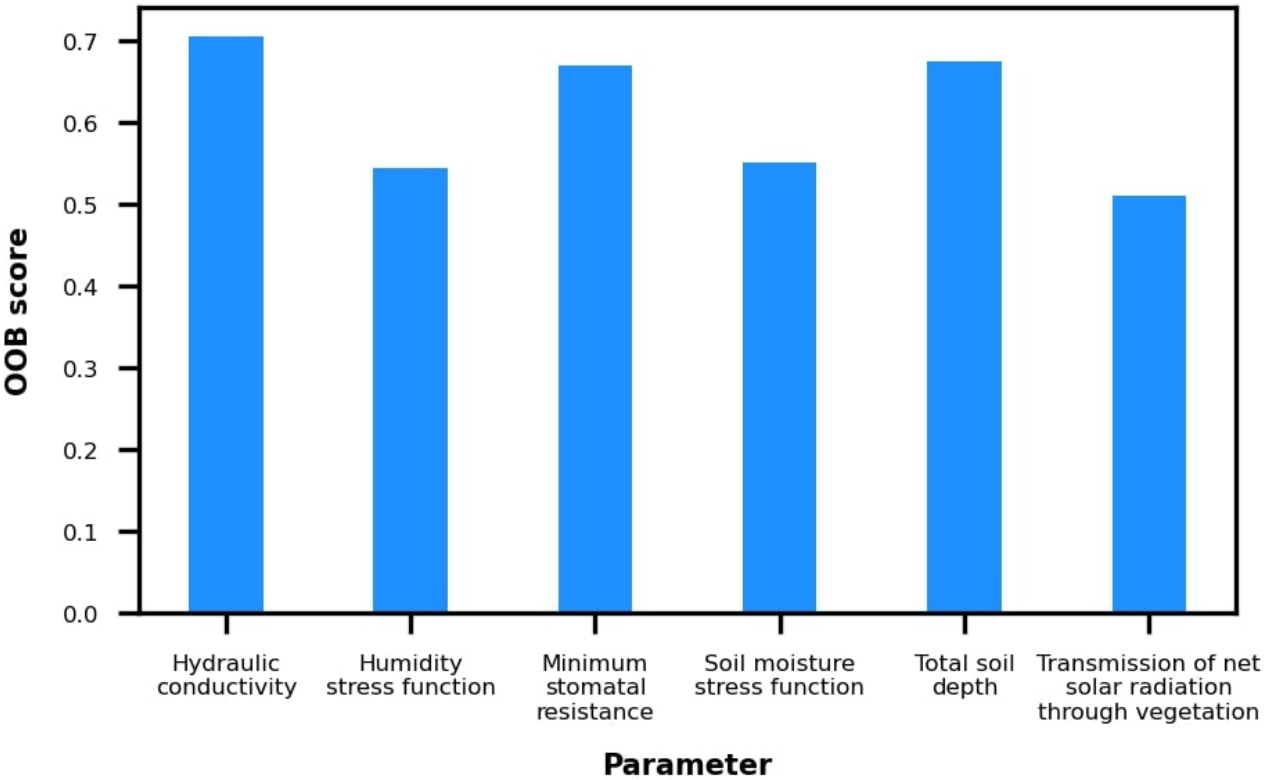

Figure S14. Model performance (OOB estimate of R^2) in the trained RF for the considered six soil and vegetation related model parameters. Higher OOB means the RF can well explain the spatial pattern of model parameters.

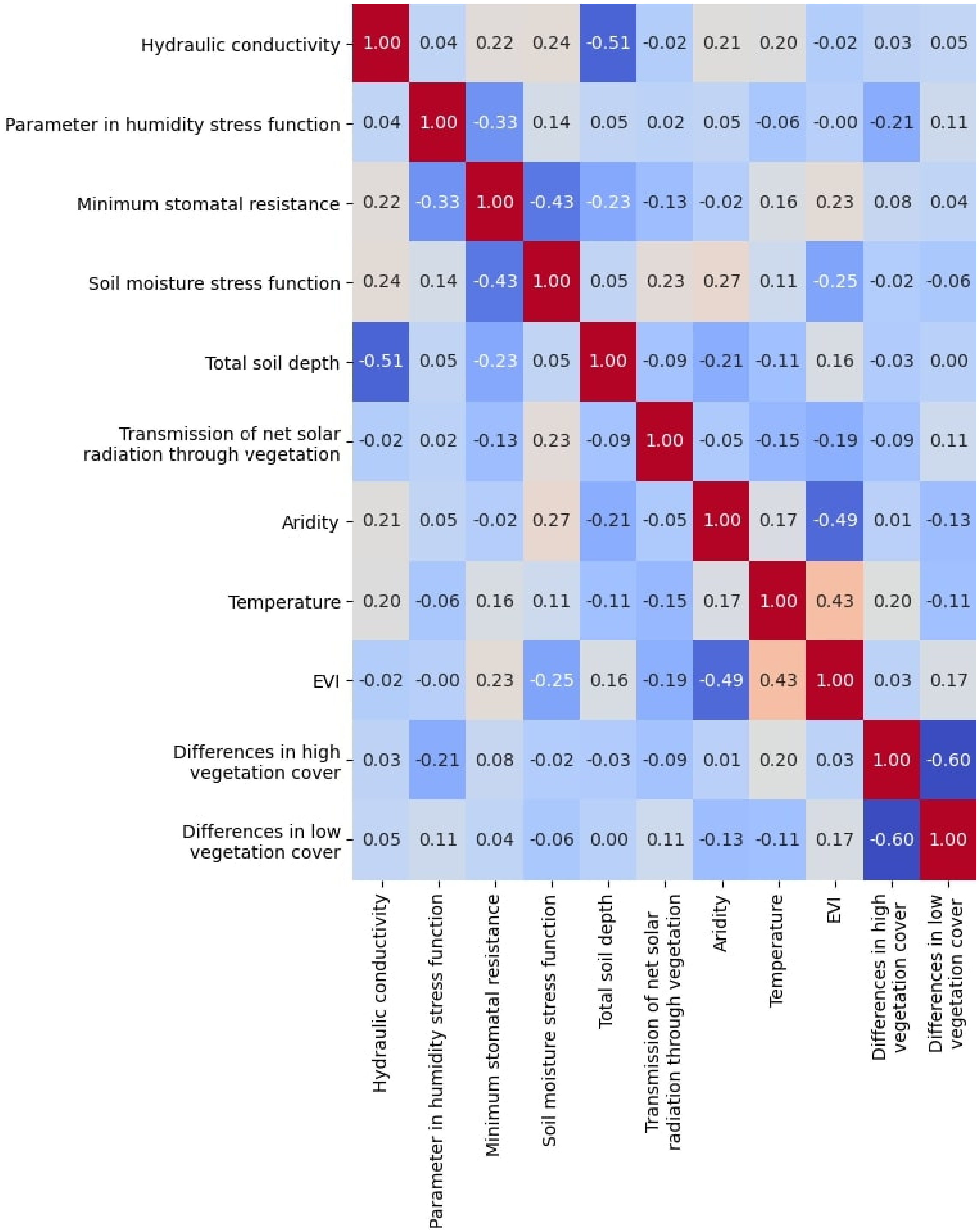

Figure S15. Spearman cross-correlation matrix among the 11 predictors used in the RF models to predict the calibrated parameter values.

References

Gelaro, R., McCarty, W., Suárez, M. J., Todling, R., Molod, A., Takacs, L., ... Zhao, B. (2017). The Modern-Era Retrospective Analysis for Research and Applications, version 2 (MERRA-2). *Journal of Climate*, *30*(14), 5419 - 5454. doi: 10.1175/JCLI-D-16-0758.1

Jung, M., Koirala, S., Weber, U., Ichii, K., Gans, F., Camps-Valls, G., ... Reichstein, M. (2019). The FLUXCOM ensemble of global Land-Atmosphere energy fluxes. *Scientific Data*, *6*. doi: 10.1038/s41597-019-0076-8

Martens, B., Miralles, D. G., Lievens, H., van der Schalie, R., de Jeu, R. A. M., Fernández-Prieto, D., ... Verhoest, N. E. C. (2017). GLEAM v3: satellite-based land evaporation and root-zone soil moisture. *Geoscientific Model Development*, *10*(5), 1903–1925. doi: 10.5194/gmd-10-1903-2017

O, S., & Orth, R. (2021). Global soil moisture data derived through machine learning trained with *in-situ* measurements. *Scientific Data*, *8*. doi: 10.1038/s41597-021-00964-1